Journal of The Electrochemical Society

The Electrochemical Society
Advancing solid state & electrochemical science & technology

OPEN ACCESS

A Manganese-Doped Barium Carbonate Cathode for Alkaline Batteries

To cite this article: Benjamin Hertzberg *et al* 2014 *J. Electrochem. Soc.* **161** A835

View the article online for updates and enhancements.

This content was downloaded from IP address 137.83.217.148 on 23/05/2020 at 09:30

A Manganese-Doped Barium Carbonate Cathode for Alkaline Batteries

Benjamin Hertzberg,[a] Lev Sviridov,[b] Eric A. Stach,[c] Tanya Gupta,[a] and Daniel Steingart[a,*,z]

[a]*Princeton University, Mechanical and Aerospace Engineering Department, Andlinger Center for Energy & the Environment, Engineering Quadrangle, Princeton, New Jersey 08544, USA*
[b]*Hunter College, Honors College Office, New York, New York 10065, USA*
[c]*Brookhaven National Laboratory, Center for Functional Nanomaterials,Upton, New York 11973-5000, USA*

MnO2-Zn alkaline batteries are one of the most common modern forms of primary battery, due to their relatively high energy density and low cost per kilowatt-hour. Additionally, unlike many other types of primary battery, alkaline cells can theoretically be recharged. Their low cost per kilowatt-hour makes them potentially ideal for applications such as sustainable energy storage or peak demand shaving. However, a phase transformation that occurs in MnO2 after reduction by more than one electron converts it into the electrochemically inactive Mn3O4 phase. This limits the total depth of discharge of the cell significantly. We report the synthesis of a novel electrode material, manganese-doped witherite, for rechargeable alkaline batteries produced by a simple hydrothermal process. The material has been studied via X-ray diffraction and electroanalytical techniques. We show that unaltered witherite has poor electrochemical properties, and that this new material has high capacity and rate capability, even under deep discharge conditions, superior to conventional manganese dioxide.
© The Author(s) 2014. Published by ECS. This is an open access article distributed under the terms of the Creative Commons Attribution Non-Commercial No Derivatives 4.0 License (CC BY-NC-ND, http://creativecommons.org/licenses/by-nc-nd/4.0/), which permits non-commercial reuse, distribution, and reproduction in any medium, provided the original work is not changed in any way and is properly cited. For permission for commercial reuse, please email: oa@electrochem.org. [DOI: 10.1149/2.083405jes] All rights reserved.

Manuscript submitted November 12, 2013; revised manuscript received March 27, 2014. Published April 11, 2014.

Manganese-zinc primary batteries, which use electrolytic manganese dioxide (EMD) as a cathode material, are one of the most common power sources for electronic devices today. Rechargeable manganese-zinc batteries have very high theoretical capacity and energy density, coupled with very low cost, and are potentially suitable for a wide range of applications, including renewable energy storage and other grid applications, due to its high capacity, ionic conductivity, and low cost.[1]

When deposited electrolytically, EMD forms the γ-MnO_2 phase, an intergrowth of pyrolusite and ramsdellite phases. This phase is characterized by a high density of tunnel-like structures that permit the easy transfer of ions into the bulk of the material, accounting for its moderate ionic conductivity, while the intergrowth of different phases produces high electronic conductivity.[2] During discharge reactions involving more than 0.5 e^-/Mn, γ-MnO_2 can transform into birnessite, a manganese dioxide phase which has very low ionic conductivity.[3,4]

Local potential gradients can trigger this transformation at electrode averaged depths of discharge as low as 20%, depending on the construction of the electrode, causing the formation of small amounts of electrochemically inactive phases. Even these small inactive particles can lead to uneven potential distributions throughout the cell, accelerating the eventual failure of the battery. This is a major failure mode of all rechargeable cells which use EMD as a cathode material.[5] Limiting the depth of discharge of the cell permits thousands of cycles, but significantly reduces the overall capacity of the cell.[6]

Varying the Mn stoichiometry, the cation vacancy fraction, the surface area, and the content of pyrolusite has no impact on the long-term cyclability of the cell, as crystallographic changes produced by cycling dominate the system.[7] Attempts to modify the synthesis process, including adding surfactants to the electrodeposition bath and using pulse deposition rather than constant current to deposit EMD, have shown little effectiveness in increasing depth of discharge.[8,9] Hydrothermal methods have also been used to produce MnO_2 with improved electrochemical stability. These materials are typically formed of δ-MnO_2, or birnessite.[10–15] While birnessite nanostructures have drastically increased depth of discharge in half-cells, the addition of zincate ions to the electrolyte from the zinc anode in a full cell causes a rapid transition from birnessite to the relatively inactive hetaerolite phase. This makes these types of hydrothermally produced nanostructures impractical for full cells.[16]

Alternative methods include MnO_2-C composites[17–19] and doping MnO_2 with materials such as Bi, Ba, Ti, or Ni.[20–24] These modified materials have increased depth of discharge, and Bi and Ba doped materials in particular have high performance. However, doping has yet to solve the problem of Zn poisoning - when cycled in an electrolyte containing zinc ions, doped cathodes still form electrochemically inactive heteraeolite.[25]

In this work, a manganese bearing cathode material been produced using a simple one-step hydrothermal process. The material is shown to be $BaMn_{0.51}C_{0.49}O_3$, with a structure similar to the witherite crystal structure typical of $BaCO_3$. While pure $BaCO_3$ is electrochemically inactive, manganese substitution creates a high degree of electrochemical activity. Additionally, this material has superior rate capability and cyclability compared to gamma MnO_2 under similar discharge conditions, with comparable cost, and has never before been described in the literature. Further, it can be used as a drop-in replacement for EMD in existing alkaline battery technologies. This approach can potentially be modified to create a wide range of potential new electrochemically active oxides with unique properties.

Experimental

Synthesis process.— Manganese-doped witherite was synthesized via a one-step hydrothermal process. Potassium permanganate (Sigma-Aldrich), barium chloride dihydrate (Sigma-Aldrich), and acetylene black (Fisher Scientific) were used as precursors. $KMnO_4$ and $BaCl_2$*$2H_2O$ were added to 400 mL of H2O in a round-bottomed flask to form a 0.1 M solution each of $KMnO_4$ and $BaCl_2$. 2 g of carbon black were added. This solution was then heated to 100°C and refluxed for approximately 4 hours, after which all of the manganese had been consumed, as indicated by the disappearance of the violet coloration of the solution. The resulting solid was separated from the solution by vacuum filtration, then further dried at 90°C for 24 hours in air to remove excess water. Thermo-gravimetric analysis shows that the water of hydration is approximately 28.69% of the total mass. The total yield of material from our synthesis is 9.3825 g, which indicates that all of the Mn has been consumed in the production of the composite.

Electron microscopy.— Scanning electron microscopy micrographs were collected using a Zeiss Supra 55 field emission Scanning Electron Microscope. Image collection was performed under high vacuum at a working distance of 2.5 mm and a voltage of 5 kV.

*Electrochemical Society Active Member.
zE-mail: steingart@princeton.edu

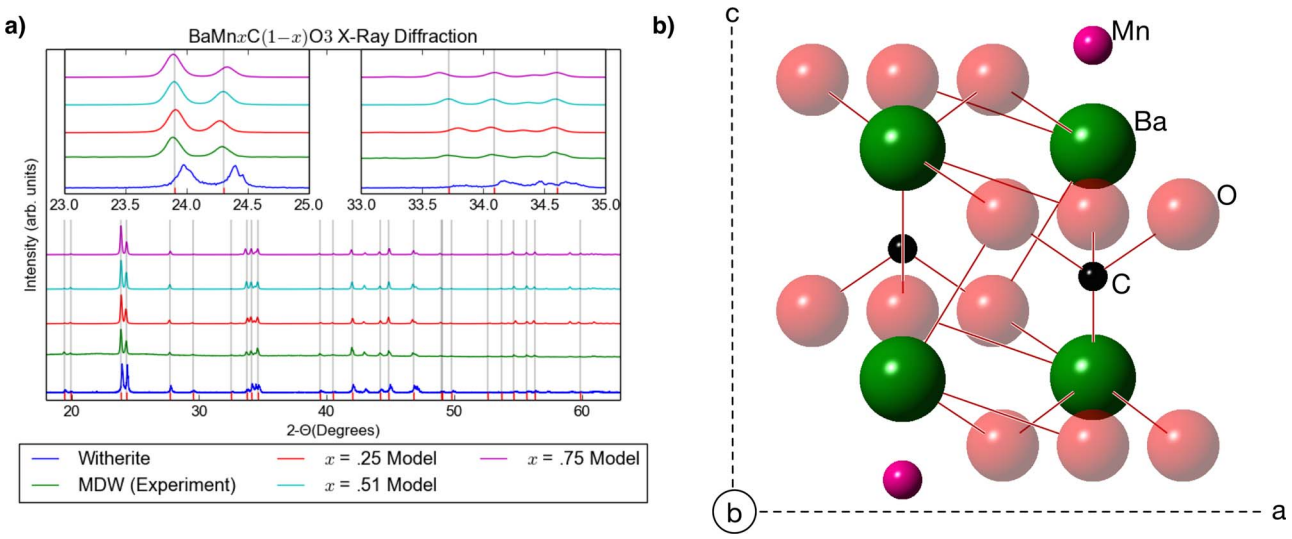

Figure 1. a) XRD spectra of manganese-doped witherite. The bottom (blue) line represents standard witherite, the top (green) line represents the Rietveld refinement fit, and the vertical (gray) lines show the peak positions indicated by the x = .51 model. b) Proposed structure of manganese-doped witherite.

The Energy Dispersive X-ray spectroscopy (EDAX) was performed using the same instrument at a working distance of 8.5 mm. TEM and ADF-STEM was collected using a FEI Titan 80–300 Environmental Transmission Electron Microscope at a voltage of 300 kV. ADF-STEM data collection was aperture-limited to 60 mRad.

XRD methodology.— The X-ray Diffraction (XRD) data were collected using a PANalytical X'Pert Pro powder diffraction instrument. The X-rays were generated using a Philips high intensity ceramic sealed tube. The incident beam is passed through Soller slits of 0.04 radians and through a divergence slit of 1 degree and a mask of 10 mm slit size. The diffracted beam passed through the PIXcel1D detector collecting the data generated from only the Cu Ka1 with a wavelength of 1.5405Å. The data suitable for Rietveld analysis[Rietveld, 1969 #32] were collected with a step size of $\Delta 2\theta = 0.0016^\circ$ over an angular range of $5 \leq 2\theta/\text{deg} \leq 125$.[28] The data were analyzed using the General Structure Analysis System (GSAS) program suite (Larson, A.C. LAUR 86–748; Los Alamos National Laboratories: 1994).

X-ray photoelectron spectroscopy.— High-resolution XPS (HR-XPS) measurements were performed with a Scienta ESCA-300 system with a 7.5 kW rotating anode monochromatic Al Ka X-ray source. The material was powdered, applied to a carbon tape-coated substrate, and analyzed under UHV conditions. Peak deconvolution and integration was accomplished via the Fityk software.[29]

Electrochemical characterization.— Electrodes were produced by taking 0.5 g of either the dried composite material or unmodified $BaCO_3$ (Sigma-Aldrich) and mixing it with 0.25 g of acetylene black (Fisher Scientific), 0.25 g of Polystyrene-Butadiene binder (LICO Technology Corp.), and water. Electrolytic manganese dioxide electrodes were produced by taking 3.0 g of electrolytic manganese dioxide (AB Grade, Tronox Corp.) and combining it with 0.6 g of graphite (Sigma-Aldrich), 0.9 g of the aforementioned binder and water. The resulting slurry was embedded into a highly porous nickel foam (MTI International). The resulting electrode was dried and then tested in a 41% KOH solution, both with ZnO (60 gL^{-1}, Sigma-Aldrich) and without. Zinc metal was used as a counter electrode, and a Hg/HgO reference electrode (Koslow Scientific Co.) was employed. Both cyclic voltammetry and standard potentiometric methods were used. In both cases, the material was cycled between −0.85 V and 0.45 V to ensure complete reaction of the structure. Our cyclic voltammetry tests used a cycling rate of .2 mVs^{-1}. Our potentiometric tests charged and discharged the material at C/20 and C/2 rates, assuming a capacity of 308 mAh/g. The material was cycled between 0.8 and 1.5 V. A 10 minute rest step was introduced between charge and discharge cycles.

Results

The X-ray diffraction spectrum for both manganese-doped and undoped witherite, as well as Rietveld refinement models of MDW with varying degrees of Mn substitution, are shown below, in Figure 1a. The X-ray pattern for the natural form of witherite is taken from Ye et al.[30] The XRD spectra appears similar to the natural mineral form of $BaCO_3$, or witherite, although a small peak shift occurs. No peaks associated with any known crystal form of MnO_2 are visible, suggesting that either MnO_2 does not form as a result of our process, or that all produced MnO_2 is amorphous in nature.

We used Rietveld refinement to analyze our XRD spectra, as further described in our Supporting Information. We constructed several different models, as shown in Figure 1a, for differing degrees of substitution in $BaC_{(1-x)}Mn_xO_3$, from x = .25 to x = .75. While the peak positions do not change significantly due to Mn substitution, relative peak height does change. Further analysis of these results showed that the composition of the material is approximately $BaC_{0.49}Mn_{0.51}O_3$. The crystal data is in good agreement with the space group of Pmcn (62) and the crystal structure is orthorhombic, much like unsubstituted $BaCO_3$, or witherite. The quality of the agreement between the theoretical model and the collected data is reflected in the Rietveld residual fit value R_{wp} value of 0.1104. The lattice parameters were calculated to be a = 5.3149(3)Å, b = 8.9076(5)Å, c = 6.4364(4)Å, also similar to unsubstituted $BaCO_3$ (a = 5.3017 Å, b = 8.90274 Å, c = 6.42761 Å).[26] The sites and occupancy fractions for each atom of the doped unit cell (x = .51) are shown below in Table I. The specific positions for each of the atoms in the structure are very similar to unmodified witherite. The C and Mn atoms are shown to both occupy the same position, at X = .25, Y = .732, Z = 0.03. This is similar to the normal position of a C atom in witherite (X = .25, Y = .7554, Z

Table I. Atomic positions, Uiso contributions, site occupancies, and Uiso contributions for $BaMn0_{.51}C_{0.49}O_3$. The (*) denotes that the Uiso for Oxygen were not refined.

Atom	Wyckoff Position	X	Y	Z	Uiso	Occupancy Fraction
Ba	4c	0.25	0.4162	0.748	9.5E-3	1
C	4c	0.25	0.732	0.03	.49	.49
Mn	4c	0.25	0.732	0.03	.49	.51
O	4c	0.25	0.908	−0.104	2.5E-2*	1
O	8d	0.487	0.669	−0.075	2.5E-2*	1

= .9231), although Z is shifted, suggesting an elongation of the unit cell.[26] The high U_{iso} (isometric displacement) values for C and Mn, compared to the other elements of the unit cell, suggest a high degree of randomness in substitution - the inserted Mn atoms are unlikely to be highly clustered.

Our analysis of the X-ray diffraction data suggests that the hydrothermally produced material has a similar crystal structure to witherite and does not resemble any known form of MnO_2. Mn atoms are fully incorporated into the witherite structure rather than occupying interstitial sites. This is not wholly unprecedented - copper, another d-block transition metal, can be incorporated into witherite as an oxidized cuprate without creating a new phase.[27] The material produced by our hydrothermal process is crystalline with a minimally distorted crystal structure. It can be described as a form of manganese-doped witherite (MDW). No other crystalline phases are detected, suggesting that any other material in the sample must be amorphous in nature, such as carbon black or amorphous MnO_2. The proposed structure is shown in Figure 1b.

Examining the crystal structure of both doped and undoped witherite, we find that the undoped witherite crystal is not a close packed structure, so even though Mn^{4+} is significantly larger than C^{4+}, the shift in the crystal structure and the XRD pattern is modest. The packing factor of normal witherite is 46.0%, while the packing factor of MDW is 46.6% - it is worth noting that the unit cell of undoped witherite is slightly smaller than that of MDW. Although Mn^{4+} is 11 times the volume of C^{4+}, carbon only occupies ~0.15% of the total unit cell volume of normal witherite, and in MDW, the combined volumes of the Mn and C atoms present in the unit cell occupy just ~0.90% of the total volume of the unit cell.

We studied this material using electron microscopy and energy-dispersive spectroscopy techniques. Scanning electron microscopy, shown in Figure 2c–2d, shows that the produced material takes form of roughly spherical nanoparticles approximately 50 to 100 nm across, much like the acetylene black precursor. These nanoparticles are aggregated both into highly porous areas that appear similar to carbon black as well as into less porous, densified areas. Energy-Dispersive X-Ray Spectroscopy further reveals elemental carbon distributed throughout the product that has not yet been converted into carbonate, suggesting that the carbon precursor is not fully consumed by the reaction. The remaining carbon black, being covered by the carbonate and highly amorphous in nature, would not be sufficiently detectable by X-ray diffraction, but would contribute to deviations from the background. This suggests that a thin film of hydrothermally synthesized material has been plated onto the surface of the carbon black nanoparticles. High-resolution TEM and annular dark-field STEM, shown in Figures 2a–2b, confirms this hypothesis. Figure 2a shows a dense layer of nanocrystalline material deposited on top of the carbon black, which has a structure and composition distinct from its substrate. The interface between the two phases is sharply defined. Figure 2b shows that the overall shape of the deposited material is closely conformal with that of the underlying substrate, and that its thickness is roughly constant over the surface of the substrate. The structural similarity of the produced material to the carbon black precursor suggests that the shape of the original reactants is indeed preserved by the hydrothermal synthesis process.

In order to confirm our hypothesis regarding the composition of the material, we used X-ray photoelectron spectroscopy (XPS) to study the valence and bond states of the atomic components of MDW, and to compare our results to standard XPS spectra of both $BaMnO_3$ and $BaCO_3$.[31,32] Our results are shown in Figure 3. Figure 3a, the Ba 3d5/2 spectrum, shows a single peak which can be deconvoluted to reveal two separate peaks, corresponding closely to the characteristic Ba3d5/2 peaks of $BaCO_3$ and $BaMnO_3$, at 780.05 and 779.43 eV respectively. This indicates that both Ba-C-O and Ba-Mn-O bonds are present in this material, and therefore that the existing manganese is incorporated directly into the witherite structure, rather than existing interstitially or as amorphous inclusions. Integration of the Ba-C-O and Ba-Mn-O peak areas shows that 54.5% of all Ba atoms in MDW are bonded to Mn-O groups, which is very close to the 51% substitution we calculated based on our Rietveld refinement results. Figure 3b, the O1s spectrum, shows a more complex profile, but can be deconvoluted to reveal the characteristic BaCO3 peak at 531.0 eV and the characteristic BaMnO3 peaks at 529.7 and 531.8 eV, showing that O atoms are attached to both Mn and C atoms in this structure. Finally, Figure 3c, the Mn2p3/2 spectrum, corresponds extremely closely to the standard model of $BaMnO_3$, with characteristic peaks at 642.6, 644.7, 653.73, and 664.14 eV.[31] Overall, the XPS data strongly indicate that O atoms are bonded to both Mn and C atoms in nearly equal proportions, and therefore that the Mn atoms are well integrated into the witherite structure. Additionally, they suggest that the valence

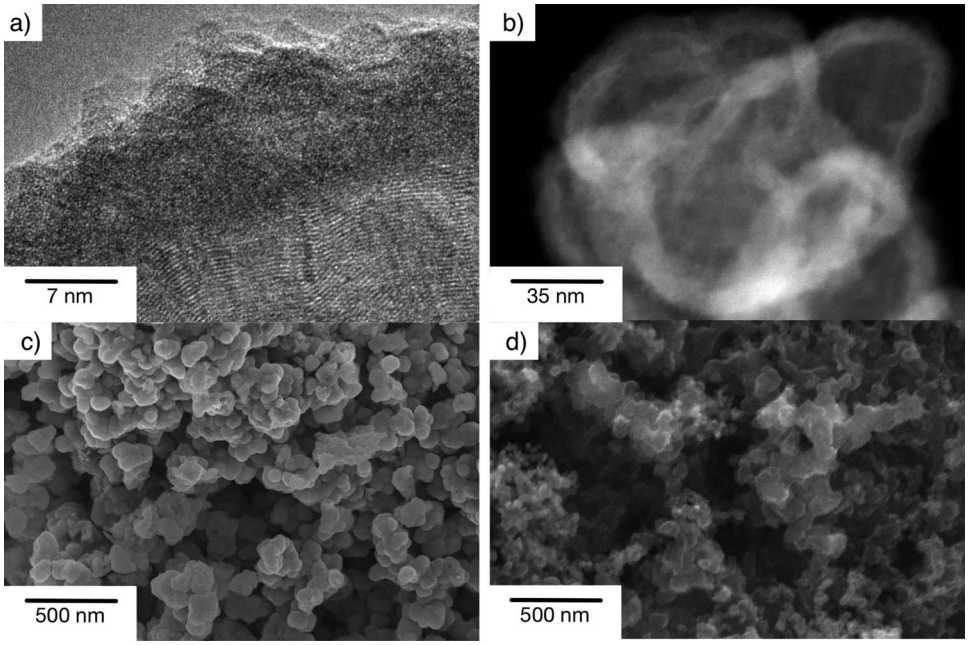

Figure 2. a) High-resolution TEM of MDW on acetylene black; b) high-resolution ADF-STEM of MDW on acetylene black; c) Electron micrograph of MDW on acetylene black; d) Electron micrograph of acetylene black.

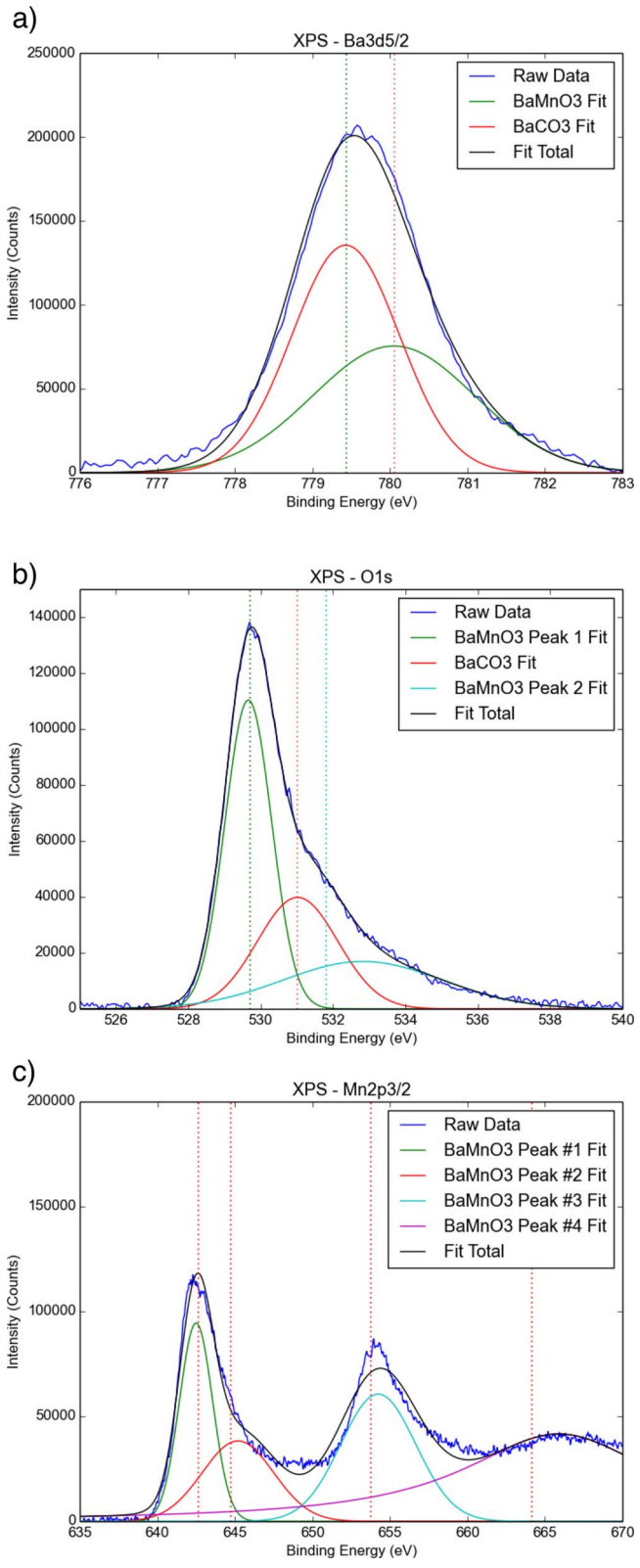

Figure 3. X-ray photoelectron spectroscopy of BaMn0.51C0.49O3. a) Ba3d5/2 spectrum; b) O1s spectrum; c) Mn2p3/2 spectrum.

state of Mn atoms in MDW is very similar to that of Mn in $BaMnO_3$, as would be expected if Mn atoms were substituted onto C sites in the witherite crystal structure.

Mn atoms are fully incorporated into the witherite structure rather than occupying interstitial sites. This is not wholly unprecedented - copper, another d-block transition metal, can be incorporated into witherite as an oxidized cuprate without creating a new phase.[27] However, in that case the structure is a perovskite rather than an aragonite group material. Transition metal substitution onto carbon sites in aragonite-type materials is unprecedented, to the best of our knowledge. We plan to further validate and examine this structure, and other doped carbonates, in the near future.

Electrochemical Performance

Following characterization, we analyzed electrodes made using both our sample and pure barium carbonate using cyclic voltammetry (CV) methods, as described in the supporting information. Our results are shown below in Figure 4a. We see that barium carbonate has little to no electrochemical activity, with negligible current density. The specific current produced by cycling our composite material has much higher specific current. Manganese-doped witherite shows a broad two-electron reduction peak at $-0.7 < V < -0.4$, and three separate oxidation peaks at $V = -0.2, -0.05$, and 0.30. It also shows consistent electrochemical performance after the 1st cycle - the specific reduction current and peak shape of the 2nd through 5th cycles remains stable, and the specific oxidation current and peak shape only diminishes slightly with increasing cycles. This suggests excellent structural stability. Cyclic voltammetry of the material in 2M NaCl and KCl electrolyte (not shown) shows no evidence of intercalation reactions, suggesting strongly that proton intercalation is the charge storage mechanism. We also charged and discharged both electrolytic manganese dioxide and the composite material at a rate of C/20 (assuming a capacity of 616 mAh/g, as per the theoretical value for MnO_2). These results are shown below in Figure 4b. Electrolytic manganese dioxide shows a capacity of ~260 mAh/g, while MDW shows much higher capacity at the same rate, with a maximum capacity of 360 mAh/g. MDW also shows significantly higher charge capacity than EMD, suggesting that the material has a more reversible charge storage mechanism. By comparison, electrolytic manganese dioxide shows virtually no charge capacity, as a result of the microstructural changes described previously. Figures 4c–4d show the results of our charge & discharge cycling of both MDW and EMD at C/20 and C/2 rates. While both MDW and EMD lose capacity with cycling, MDW loses capacity much more slowly than EMD - EMD loses virtually all of its capacity after the first cycle, while MDW retains reasonable capacity for many more cycles. MDW also retains greater capacity when cycled at C/2 rates than EMD does −160 vs 120 mAh/g, indicating superior rate capability.

Conclusions

We have developed a novel material that shows great promise as a drop-in replacement for electrolytic manganese dioxide. This material, produced via a simple hydrothermal process, appears to be isostructural with barium carbonate. Refinement of the X-ray diffraction spectra of the material suggests that it can be described as a form of manganese-doped witherite ($BaCO_3$), with roughly 50:50 substitution of manganese atoms on carbon sites. Additionally, the synthesis process appears to preserve the shape of the original carbon precursor material. The material produced exhibits high capacity and rate capability compared to normal manganese dioxide, with a first-cycle capacity of ~360 mAh/g, as well as rechargeability even after deep discharge. This material requires further investigation to determine the specific crystalline and amorphous phases produced by the synthesis process and its exact charge storage mechanism. In addition to its promise as a battery electrode material, manganese-doped witherite is structurally similar to some other materials studied as high-temperature superconductors or colossal magnetoresistive materials, such as copper-substituted barium carbonate. The high performance of manganese-doped witherite suggests that some of these materials may also be potential candidates for electrode materials. We will investigate this material and similar systems further in the future.

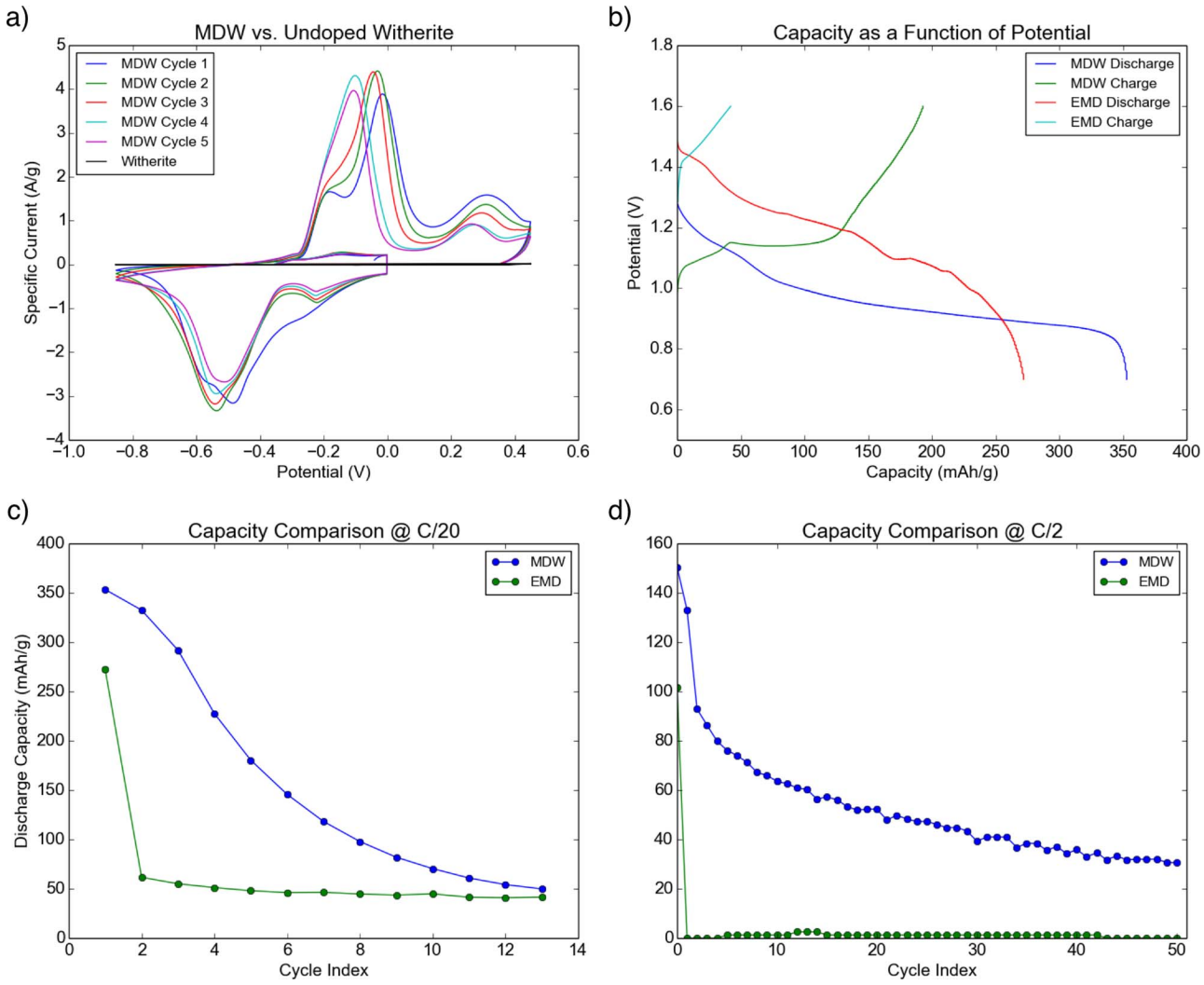

Figure 4. a) Cyclic voltammetry of barium carbonate and manganese-doped witherite; b) Charging and discharging of electrolytic manganese dioxide and MDW at a C/20 rate; c) Discharge capacity of MDW and EMD samples cycled against zinc at a C/20 rate; d) Discharge capacity of MDW and EMD samples cycled against zinc at a C/2 rate.

Supplemental information is available upon request to the corresponding author.

Acknowledgments

This work was made possible by the trust and stewardship of the NSF and DOE. We thank Joshua Gallaway, Abhinav Gaikwad and Tal Sholklapper for their advice and consultation, and Xiaobo He for his assistance in X-ray photoelectron spectroscopy. Research carried out in part at the Center for Functional Nanomaterials, Brookhaven National Laboratory, which is supported by the DOE, Office of Basic Energy Sciences, under contract DE-AC02-98CH10886. Tanya Gupta and Dan Steingart were partially supported by NSF CMMI 1031208.

Abbreviations

EMD, Electrolytic manganese dioxide; MDW, Manganese doped witherite; CV, Cyclic voltammetry.

References

1. D. Linden and T. Reddy, *Handbook of batteries*, McGraw-Hill, New York, USA (2002).
2. Y. Chabre and J. Pannetier, *Prog. Solid State Chem.*, **23**(1), 1 (1995).
3. A. Kozawa and J. F. Yeager, *J. Electrochem. Soc.*, **115**, 1003 (1968).
4. D. Y. Qu, B. E. Conway, L. Bai, Y. H. Zhou, and W. A. Adams, *J. Appl. Electrochem.*, **23**, 693 (1993).
5. C. Mondoloni, M. Laborde, J. Rioux, E. Andoni, and C. Lévy-Clément, *J. Electrochem. Soc.*, **139**, 954 (1992).
6. Y. Shen and K. Kordesch, *J. Power Sources*, **87**, 162 (2000).
7. M. R. Bailey and S. W. Donne, *Electrochimica Acta*, **56**, 5037 (2011).
8. M. Ghaemi, L. Khosravi-Fard, and J. Neshati, *J. Power Sources*, **141**, 340 (2005).
9. H. Adelkhani, M. Ghaemi, and S. M. Jafari, *J. Power Sources*, **163**, 1091 (2007).
10. Y. Yang, L. Xiao, Y. Zhao, and F. Wang, *Internat. J. Electrochem. Sci.*, **3**, 67 (2008).
11. W. Li, Q. Liu, Y. Sun, J. Sun, R. Zou, G. Li, X. Hu, G. Song, G. Ma, J. Yang, Z. Chena, and J. Hu, *J. Mater. Chem.*, **22**, 14864 (2012).
12. J. Ni, W. Lu, L. Zhang, B. Yue, X. Shang, and Y. Lv, *J. Phys. Chem. C*, **113**, 54 (2008).
13. J. H. Zeng, Y. F. Wang, Y. Yang, and J. Zhang, *J. Mater. Chem.*, **20**, 10915 (2010).
14. R. Han, S. Xing, Z. Ma, Y. Wu, and Y. Gao, *J. Mater. Sci.*, **47**, 3822 (2012).
15. X. Duan, J. Yang, H. Gao, J. Ma, L. Jiao, and W. Zheng, *CrystEngComm*, **14**, 4196 (2012).
16. M. A. Dzieciuch, N. Gupta, and H. S. Wroblowa, *J. Electrochem. Soc.*, **135**, 2415 (1988).
17. P. Bezdička, T. Grygar, B. Klápště, and J. Vondrák, *Electrochimica Acta*, **45**, 913 (1999).
18. X. Huang, H. Yue, A. Attia, and Y. Yang, *J. Electrochem. Soc.*, **154**, A26 (2007).
19. A. E. Fischer, K. A. Pettigrew, D. R. Rolison, R. M. Stroud, and J. W. Long, *Nano Letters*, **7**, 281 (2007).
20. L. Binder, W. Jantscher, F. Hofer, and G. Kothleitner, *J. Power Sources*, **70**, 1 (1998).
21. V. K. Nartey, L. Binder, and A. Huber, *J. Power Sources*, **87**, 205 (2000).
22. M. R. Bailey, J. A. Denman, B. V. King, and S. W. Donne, *J. Electrochem. Soc.*, **159**, A158 (2011).

23. D. Im, A. Manthiram, and B. Coffey, *J. Electrochem. Soc.*, **150**, A1651 (2003).
24. V. Raghuveer and A. Manthiram, *Electrochem. Comm.*, **7**, 1329 (2005).
25. X. Li, Z. Li, T. Xia, H. Dong, Y. Song, and L. Wang, *J. Phys. Chem. Sol.*, **73**, 1229 (2012).
26. J.P.R. de Villiers, *The American Mineralogist*, **56**, 758 (1971).
27. F. C. Matacotta, G. Calestani, A. Migliori, P. Nozar, P. Scardi, O. Greco, P. Ricci, A. Tomasi, and K. A. Thomas, *J. Solid State Chem.*, **129**, 165 (1997).
28. H. M. Rietveld, *J. Appl. Crys.*, **2**, 65 (1969).
29. M. Wojdyr, *J. Appl. Crys.*, **43**(5), 1126 (2010).
30. Y. Yu, J. R. Smyth, and P. Boni, *American Mineralogist*, **97**(4), 707 (2012).
31. K. B. Garg, M. Heinonen, P. Nordblad, S. D. Dalela, N. Panwar, V. Sen, S. K. Agarwal, and N. Sharma, *Inter. J. Mod. Phys. B*, **25**(9), 1235 (2011).
32. C. D. Wagner, *Handbook of x-ray photoelectron spectroscopy*. Physical Electronics Division, Perkin-Elmer Corp., 1979.